Hindawi
Journal of Chemistry
Volume 2023, Article ID 4798837, 11 pages
https://doi.org/10.1155/2023/4798837

Research Article

Magnetic Mesoporous Silica Nanoparticles Functionalized with 5,5′-Dithiobis(2-Nitrobenzoic Acid) for Highly Efficient Removal of Organic Dyes from Contaminated Water

Abeer Beagan, Shrooq Khibari, and Abdullah Alswieleh

Department of Chemistry, College of Science, King Saud University, P.O. Box 2455, Riyadh 11451, Saudi Arabia

Correspondence should be addressed to Abeer Beagan; abeagan@ksu.edu.sa and Abdullah Alswieleh; aswieleh@ksu.edu.sa

Received 28 February 2023; Revised 30 May 2023; Accepted 28 August 2023; Published 4 September 2023

Academic Editor: Adrian Saura-Sanmartin

The removal of organic pollutants has become an increasingly important environmental concern. In recent years, there has been significant research into the use of nanomaterials for removing organic dyes in single-component systems. In this study, magnetic mesoporous silica nanoparticles (magnetic MSNs) were prepared with an average particle size of 170 nm. Iron oxide nanoparticles (20 nm) were embedded within the mesoporous silica structure. These nanoparticles were functionalized with amine, derivatized with thiol, and then reacted with 5,5′-dithiobis-(2-nitrobenzoic acid) (DTNB). The presence of DTNB molecules attached to the surface was confirmed by FTIR spectra, as evidenced by the appearance of peaks at ~1528 cm^{-1} and ~1365 cm^{-1}. The nanoadsorbents demonstrated high removal efficiency for bromothymol blue (BT) and methyl orange (MO) at a pH below 5, with a maximum adsorption capacity of 139.27 mg/g and 101.62 mg/g for BT and MO, respectively. The linear regression coefficient value suggested that the adsorption of BT and MO onto magnetic MSNs-DTNB followed the Langmuir isotherm and second-order process. Overall, these findings suggest that magnetic MSNs-DTNB could be a promising nanoadsorbent for removing organic pollutants from contaminated water sources.

1. Introduction

The significant advancement of industry worldwide has resulted in the discharge of numerous forms of contaminants, including organic dyes, into the water. The consequences of this are adverse impacts on both the natural surroundings and human well-being [1–5]. Dyes are released into the environment from various sources such as industrial processes, textile manufacturing, and domestic activities such as laundry and cloth dyeing. These pollutants can harm aquatic life, decrease water quality, and pose a risk to human health when discharged into water [6, 7]. Most organic dyes are toxic and nonbiodegradable [8, 9]. Hence, it is necessary to dispose of them from wastewater before discharging them into water bodies and must be removed from wastewater before it can be discharged into waterways.

Researchers have focused on developing processes to remove organic dyes from wastewater. Various methods encompassing physical, chemical, and biological approaches have been devised to remove dyes from contaminated water. Physical techniques employ sorbents to extract dyes from water. Chemical techniques include coagulation/flocculation, oxidation, and ion exchange. Biological techniques utilize microorganisms to break down or modify the dyes into less harmful substances [10–15]. Adsorption is regarded as an economical and highly effective process for eliminating organic dyes from polluted water [16, 17]. Different materials have been used as adsorbents, such as metal-organic frameworks (MOFs) [18], activated carbon (AC) [19], metal-doped porous carbon materials [20], bioadsorbent [21], and mesoporous materials [22, 23].

Mesoporous silica nanoparticles (MSNs) have been developed as new inorganic materials for various applications, including environmental applications, due to their large specific surface area, pore volume, and high chemical and thermal stability. Different types of MSNs can be

synthesized based on the pore and particle size, surface area, and preparation method. For example, MCM-41 and MCM-48 are characterized by a 3-dimensional cubic pore structure, which can usually be prepared in basic media in the presence of an ionic template [24, 25]. SBA-15 particles have a similar hexagonal structure to MCM-41, which can be prepared using an amphiphilic block copolymer under acidic conditions [26, 27].

Magnetic mesoporous silica nanoparticles (magnetic MSNs) are a class of nanomaterials that consist of a core of iron oxide coated with a porous shell of silica. Iron oxide nanoparticles (Fe_3O_4 NPs) are characterized by their strong magnetic properties, high specific surface area, low toxicity, and high biocompatibility [28–31]. Despite these advantages, several disadvantages have been noticed in magnetic nanoparticles, such as aggregation and oxidation in air, which limit their use [32]. To overcome these drawbacks, coating magnetic NPs with a silica shell can enhance their stability and prevent their aggregation [33, 34]. Magnetic MSNs have attracted great interest and significant use in a number of fields, such as biomedicine [35, 36], drug delivery [37], sensing [38], stimulation [39], separation [40], printing [41], and water treatment [42]. Magnetic MSNs can be used as adsorbent materials to remove dyes due to their unique characteristics, such as high surface areas and ease of separation using an external magnetic field [43]. However, the use of unmodified surface MSNs is limited in application, and therefore, it is necessary to modify the surface of MSNs to increase their adsorption capacity and stability. Modification of surface MSNs with different polymers [44, 45] or functional groups, such as thiol [46], sulfonic acid [22, 47], carboxylic acids [48], and amino acid [49–51], could increase the adsorption capacities. For instance, MSNs modified with cysteine (MSN-Cys) were prepared as a nanosorbent to remove MB from an aqueous solution at different pH. The adsorption isotherm was fitted with the Freundlich model, and the kinetics of MB adsorption on MSN-Cys was found to fit a pseudo-second-order kinetic model, with an adsorption capacity of 140 mg/g [49]. Beagan developed a nanosorbent by coating Fe_3O_4 NPs with MSNs and modified with aspartic acid via a hydrophobic linker to effectively remove MB dye from contaminated water, and the maximum adsorbed amount of MB was estimated to be 135 mg/g at 200 mg/L MB concentration and 80 minutes' contact time [52]. Magnetic MSNs modified with poly(2-methacryloyloxy) ethyl trimethylammonium chloride brush were found to be highly efficient in removing MO and bromothymol blue (BT) dyes from contaminated water, with a removal efficiency of 100% at 100 ppm and unaffected adsorption performance by pH. They could be a promising sorbent for the removal of other pollutants from water and wastewater [53].

Due to the intricate structure of dye molecules, it is crucial to remove multiple toxic dyes from contaminated water. Thus, this study aims to develop a material that employs magnetic mesoporous silica nanomaterial modified with 5,5′-dithiobis-(2-nitrobenzoic acid) (DTNB) to effectively eliminate toxic dyes from aqueous solutions (Scheme 1). The synthesis process involved the co-precipitation of ferric and ferrous salts to generate iron oxide nanoparticles. A mesoporous silica shell was then coated on the Fe_3O_4 core using tetraethyl orthosilicate (TEOS) as the source of silica and cetyltrimethylammonium bromide (CTAB) as the template. The surface of MSNs was subsequently modified with amine, followed by a reaction with ethylene sulfide and DTNB. The study investigated the impact of various parameters, such as contact time, pH, and initial dye concentration, on the adsorption efficiency of ionic dyes (bromothymol blue (BT) and methyl orange (MO)). Adsorption isotherms and kinetic models were employed to fit the experimental data.

2. Materials and Methods

2.1. Materials. Hexane (HPLC grade), ammonium hydroxide (NH_4OH, 28 wt%), cetyltrimethylammonium bromide (CTAB, 98%), 3-aminopropyltriethoxysilane (APTES, >98%), ammonium nitrate (NH_4NO_3, 99%), ethylene sulfide (98%), ethanol (HPLC grade), methanol (HPLC grade), tetraethyl orthosilicate (TEOS, 98%), methyl orange (MO, 85%), and bromothymol blue (BT, 95%) were purchased from Sigma-Aldrich, Germany. Ferric chloride (99%) and ferrous chloride (99%) were obtained from Loba Chemie, India. Ellman's reagent (5,5′-dithiobis(2-nitrobenzoic acid) (DTNB)) was acquired from vwr, England. Hydrochloric acid (HCl, 36%) was purchased from Fisher Scientific. All chemicals and reagents were used as received.

2.2. Synthesis of Magnetic Mesoporous Nanoparticles (Magnetic MSNs). For the preparation of iron oxide nanoparticles (Fe_3O_4-NPs), 50 mL of ferric chloride solution (0.98 M) was mixed with 50 mL of ferrous chloride solution (0.82 M). Then, the ammonium hydroxide (30 mL, 28 wt%) was added to the solution under N_2 gas and stirred at 85°C for 20 min. The Fe_3O_4-NPs were collected by filtration then washed for five times with deionized water and ethanol [54].

To prepare magnetic mesoporous nanoparticles, 0.5 g of Fe_3O_4-NPs were suspended in 200 mL deionized water. Then, 0.8 g of CTAB was added to the suspension, followed by the addition of 10 mL of ammonia water at 45°C. A mixture of *n*-hexane (14 mL) and TEOS (6 mL) solutions was added to the suspension. After 15 h, the solid was separated by filtration and washed five times with water and ethanol [55].

To extract the template, magnetic mesoporous nanoparticles were suspended in a solution of ammonium nitrate/ethanol (8 mg/mL). The mixture was stirred at 75°C for 6 h. Magnetic MSNs were separated and washed with ethanol four times [55].

2.3. DTNB-Modified Magnetic Mesoporous Silica (Magnetic MSNs-DTNB). Dried Fe_3O_4-MSNs were suspended in a mixture of APTES (0.3 mL) and methanol (50 mL). Then, the mixture was heated under reflux for 15 h under stirring. Magnetic MSNs-NH_2 were separated and washed six times with methanol and dried at 80°C for 3 h [55].

Magnetic MSN-NH_2 WAS suspended in 40 mL ethanol, followed by the addition of ethylene sulfide (0.5 mL). The reaction mixture was stirred for 24 h. The sample was

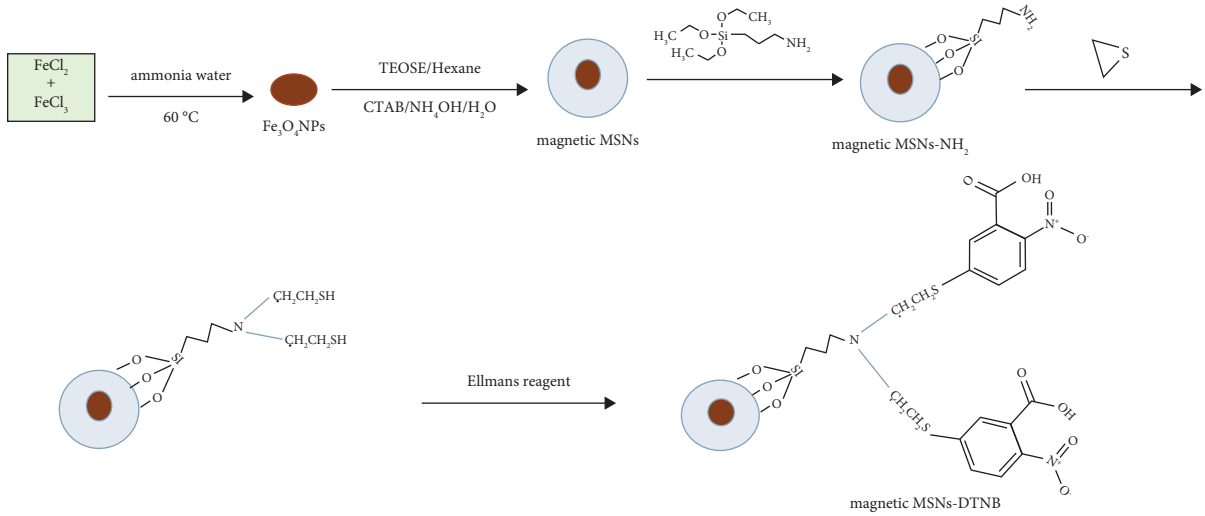

Scheme 1: Schematic representation of the synthesis route of magnetic MSNs-DTNB.

separated and washed with ethanol five times. The sample was dried at 80°C for 3 h [56].

Thiol functionalized magnetic nanoparticles were suspended in 50 mL aqueous solution (0.1 mM) of freshly prepared Ellman's reagent and left under stirring for 2 h. The sample was separated by centrifugation and washed with distilled water and ethanol five times. Finally, the magnetic MSNs-DTNB were dried at 80°C for 3 h [57, 58].

2.4. Characterization and Measurement. Topological images of Fe_3O_4 embedded in mesoporous silica nanoparticles were obtained from SEM (JEOL JSM-6380 LA, Japan) and TEM (JEOL JEM-1230, Japan). FTIR spectroscopy (Thermo Scientific Nicolet IS10, USA) was utilized in the range 4000–400 cm^{-1} to identify the chemical functional group of the nanoparticles. TGA analyzer (SII TGA 6300 thermogravimetry analyzer, Japan) was utilized with a heating rate 10°C/min. UV-vis spectrophotometer (Shimadzu UV-2600, Japan) was utilized in the adsorption study.

2.5. Dyes Adsorption Study. The adsorption study of ionic dyes onto magnetic MSNs-DTNB adsorbent was examined by varying initial concentrations of dyes, pH, and contact time. First, 500 ppm stock solutions of the dyes were prepared in the volumetric flask at different pH values. Then, the required volume of the stock solution was transferred to 100 mL volumetric flask then filled the flask to the line with DI water, making the standards by diluting the stock solution. At least 5 concentrations were taken and evaluated by UV-vis spectrophotometer to have a good calibration curve with a linear regression coefficient (R^2) value closed to 1.

The synthesized nanoparticles (10 mg) were added to 10 mL at different concentration of dyes solution and shaken at 200 rpm/min at room temperature. The adsorbent was separated by a centrifuge, and filtrates were evaluated by UV-vis spectrophotometer. The adsorption capacity was calculated by the following expression:

$$q_e = \frac{(C_o - C_e)V}{m}. \quad (1)$$

The adsorption capacity at equilibrium (mg/g) represented by q_e, while C_o and C_e, respectively, refers to the initial concentration of dyes (mg/L) and the dye concentration at equilibrium (mg/L). V and m denote the volume of the contaminated solution (L) and the quantity of nanoparticles (g), correspondingly.

2.6. Adsorption Isotherms. The adsorption isotherm helps in understanding the relationship between the amounts of dyes on the surface of nanoparticles to its concentration. The most popular models for analyzing the adsorption behavior of the nanoparticles are Freundlich and Langmuir adsorption isotherm models.

Langmuir's model assumes that the dye will be deposited on the surface of the nanoparticles in the form of a monolayer, and that the dye molecules will not interact with each other. The linear form of the Langmuir isotherm can be defined by the following equation:

$$\frac{C_e}{q_e} = \frac{1}{q_m K_l} + \frac{C_e}{q_m}, \quad (2)$$

where C_e and q_e describe the equilibrium concentration of dyes (mg/L) and the adsorption capacity at equilibrium(mg/g), respectively. q_m describes the maximum adsorption capacity of dyes onto the nanomaterials (mg/g). k_l describes the Langmuir constant representing the affinity of binding sites (L/mg).

Freundlich isotherms show that the adsorption of dye is multilayered on heterogeneous surfaces. The Freundlich model isotherm can be defined by the following equation:

$$\log q_e = \frac{1}{n}\log C_e + \log K_F, \quad (3)$$

where $1/n$ defined as the adsorption intensity and surface heterogeneity, and K_F describes the Freundlich adsorption constant $((\text{mg/g})/(\text{mg/L})^{1/n})$.

2.7. Adsorption Kinetics. The adsorption kinetics of the dyes onto nanomaterials was evaluated by using pseudo-first-order and pseudo-second-order equations, respectively.

$$\log(q_e - q_t) = \log(q_e) - \frac{K_1}{2.303}\, t, \tag{4}$$

$$\frac{t}{q_t} = \frac{1}{K_2 q_e^2} + \frac{1}{q_e}\, t, \tag{5}$$

where q_t (mg/g) is the adsorption capacity at time t. K_1 (L/min) and K_2 (g/mg·min) are the rate coefficient of pseudo-first-order and pseudo-second-order, respectively.

3. Results and Discussion

The morphological structure of surface-modified nanoparticles (magnetic MSNs-DTNB) was determined using SEM and TEM, as shown in Figure 1. As illustrated in Figure 1(a), magnetic MSNs-DTNB were almost spherical in shape, with a size ranging between 145 nm and 260 nm. The TEM image of the sample showed a dark spot in the middle of the magnetic MSNs-DTNB, which was related to iron oxide nanoparticles with an average particle size of 20 nm (Figure 1(b)). Furthermore, the magnetic MSNs-DTNB revealed a mesoporous structure, with an average pore size of 5 nm, as estimated from the TEM image. No significant difference in the particle size was observed between the SEM and TEM images.

To identify the organic molecules attached to the surface of the nanoparticles, the FTIR technique was used. As shown in the FTIR spectra in Figure 2, the broad peaks at 1250–1050 cm^{-1} and 810 cm^{-1} were attributed to the silicon-oxygen band stretching of the silica network. The FTIR spectra of magnetic MSNs with CTAB showed two peaks at ~2900 cm^{-1} and ~1430 cm^{-1}, which were assigned to the C-H stretching mode of CTAB molecules [14, 59]. After the extraction process, the peaks at ~2900 cm^{-1} and ~1430 cm^{-1} disappeared, indicating the successful removal of CTAB from MSNs. Peaks at ~2950 cm^{-1} were noticed in the FTIR of magnetic MSNs-NH_2 and magnetic MSNs-SH assigned to the C-H stretching mode of the organic layer. After the reaction with DTNB, new peaks appeared at ~1528 cm^{-1} and ~1365 cm^{-1}, which could be attributed to the nitro group stretches of DTNB molecules.

The TGA analysis was applied to investigate the weight loss of the fabricated magnetic nanoparticles, as shown in Figure 3. The weight loss in the CTAB-free magnetic MSNs sample was ca. 8% at 500°C, indicating the presence of traces of the template and ethoxy groups from TEOS. Aminopropyl groups attached to magnetic MSNs showed a weight loss of around 10% at ca. 250°C. There was no significant difference in weight loss when the particles reacted with ethylene sulfide. However, magnetic MSNs-DTNB illustrated weight loss of 20% at ca. 260°C. The gradual increase in the weight loss confirmed the successful surface modification of the magnetic MSNs.

The elemental analysis technique provided additional support for the incorporation of amine in the magnetic MSN, as well as the successful reactions with ethylene sulfide and DTNB. To quantify the amount of organic material attached to the nanoparticle surfaces, the CHN analysis was performed on Fe_3O_4-MSNs, Fe_3O_4-MSNs-NH_2, Fe_3O_4-MSNs-SH, and Fe_3O_4-MSNs-DTNB, and the results are presented in Table 1. The carbon and nitrogen concentrations in the functionalized samples were higher compared to the nanomodified sample, indicating that the particles were successfully functionalized. The Fe_3O_4-MSNs-NH_2 had an increase of approximately 7.16% in carbon concentration and 2.62% in nitrogen concentration. The same increase was observed for the Fe_3O_4-MSNs-SH sample, with an additional increase in sulfur concentration, which suggests that MSN successfully reacted with amine and ethylene sulfide. Since Fe_3O_4-MSNs-NH_2 structure does not naturally contain these elements, the increase in both carbon and nitrogen concentrations indicates successful functionalization. After DTNB attachment, the carbon and nitrogen concentrations further increased, confirming the success of the loading process.

To investigate the effect of pH on the removal efficiency of BT and MO, different pH values between 3 and 9 were selected at contact time 3 h 25°C and 100 ppm. Figure 4 shows the removal efficiency of all dyes by magnetic MSNs-NH_2 and magnetic MSNs-DTNB. It was observed that both nanoadsorbents have ca. 100% removal efficiency towards removing BT and MO at pH values below 3. Magnetic MSNs-DTNB has ca. 85% removal efficiency towards removing BT and MO at pH 5, whereas magnetic MSNs-NH_2 has ca. 100% at the same conditions. Both nanoadsorbents have removal efficiency ranged between 45 and 60% towards removing BT and MO at pH values above 7. In addition, the effects of initial dye concentrations on the removal efficiency of both dyes were examined under a pH value of 3. The findings are illustrated in Figure 4(c). When the initial dye concentration was below 100 mg/L, the decontamination efficiency did not show a significant change as the concentration increased from 25 mg/L to 100 mg/L. However, as the initial dye concentration rose from 100 mg/L to 150 mg/L, the removal efficiency gradually declined.

Langmuir and Freundlich's isotherms have been used to model the experimental adsorption data obtained at pH 5, as shown in Figure 5, and the isotherm parameters are presented in Table 2. The adsorption of BT and MO onto magnetic MSNs-NH_2 and magnetic MSNs-DTNB followed the Langmuir isotherm better than Freundlich's isotherm as indicated by the linear regression coefficient (R^2) value. The Langmuir model describes the formation of a monolayer of the organic dyes onto the surface of the adsorbents. The maximum adsorption capacity of BT and MO onto magnetic MSNs-NH_2 was found to be 115.13 mg/g and 68.92 mg/g, respectively, whereas the maximum adsorption capacity of BT and MO onto magnetic MSNs-NH_2 was found to be 139.27 mg/g and 101.62 mg/g, respectively.

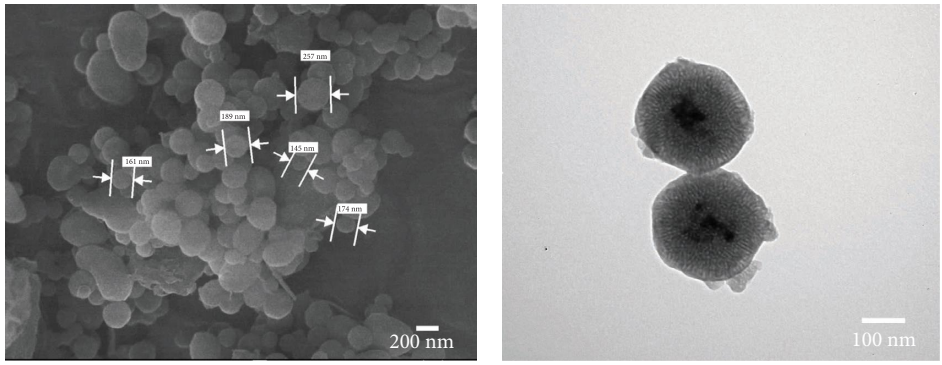

Figure 1: Topological images of Fe_3O_4 embedded in mesoporous silica nanoparticles: (a) SEM and (b) TEM.

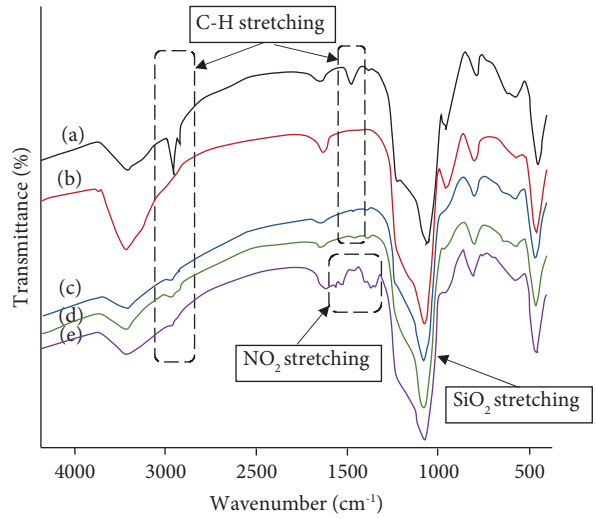

Figure 2: FTIR spectra of the synthesized nanomaterials: (a) magnetic MSNs with CTAB, (b) CTAB-free magnetic MSNs, (c) magnetic MSNs-NH_2, (d) magnetic MSNs-SH, and (e) magnetic MSNs-DTNB.

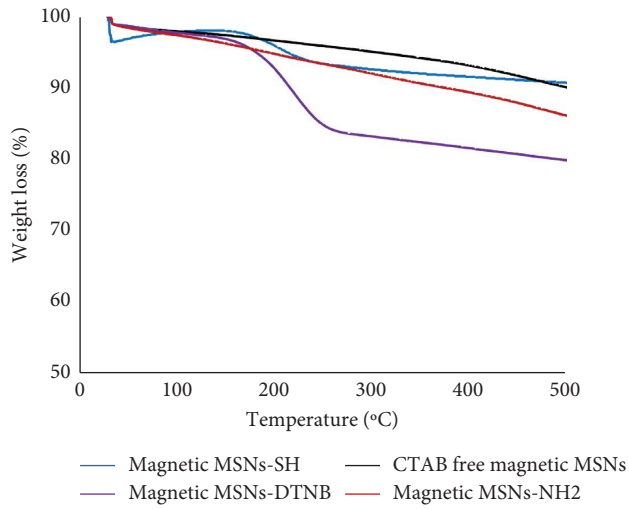

Figure 3: TGA of the synthesized nanomaterials: (black) CTAB-free magnetic MSNs, (red) Fe_3O_4-MSNs-NH_2, (blue) Fe_3O_4-MSNs-SH, and (violet) Fe_3O_4-MSNs-DTNB.

Table 1: CHN elemental analysis data for carbon, nitrogen, and hydrogen obtained from samples: Fe_3O_4-MSNs, Fe_3O_4-MSNs-NH_2, Fe_3O_4-MSNs-SH, and Fe_3O_4-MSNs-DTNB.

Materials	C (%)	N (%)	H (%)	S (%)
Fe_3O_4-MSNs	1.94	0.04	0.43	0.01
Fe_3O_4-MSNs-NH_2	7.16	2.62	2.95	0.04
Fe_3O_4-MSNs-SH	9.38	2.91	3.73	1.88
Fe_3O_4-MSNs-DTNB	13.26	4.07	4.42	1.53

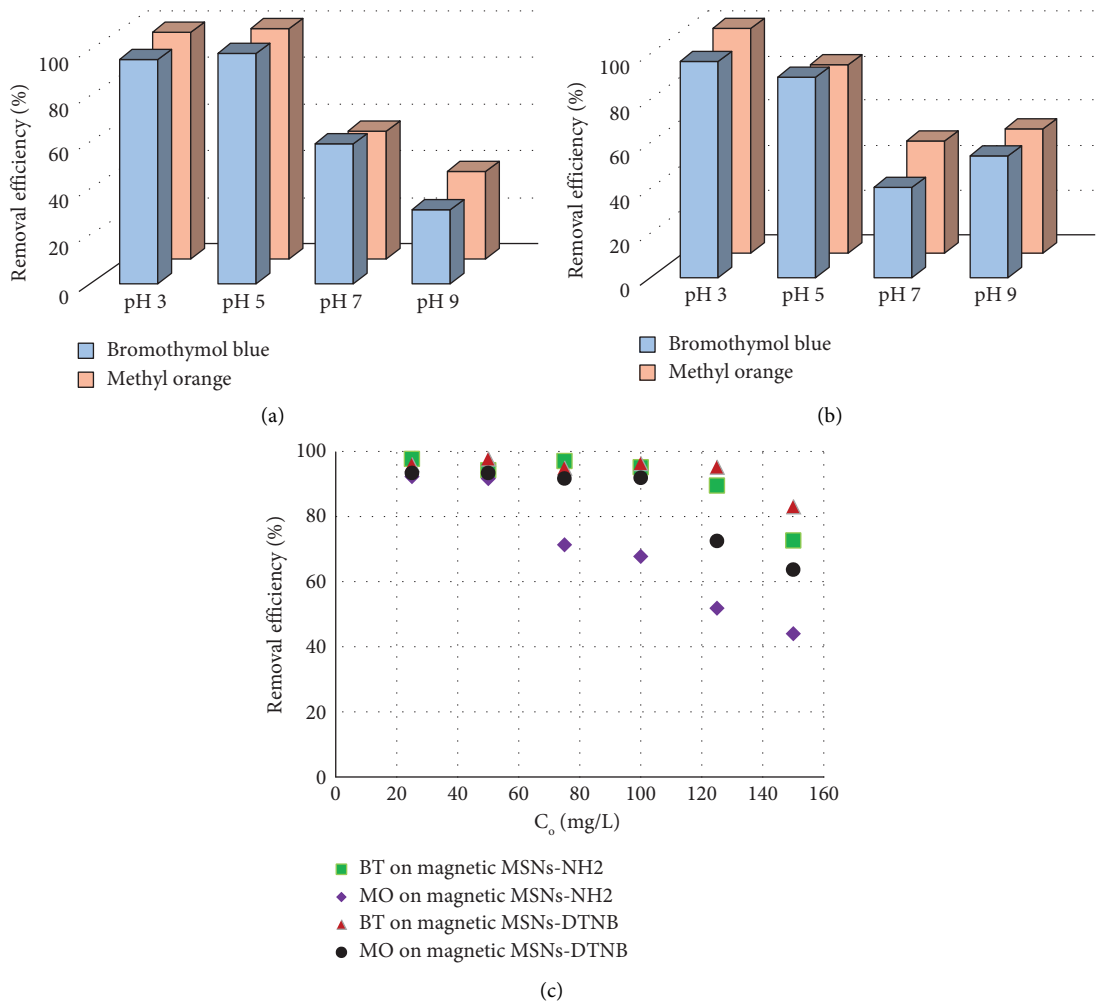

Figure 4: (a) The effect of pH media on the removal efficiency of BT and MO by magnetic MSNs-NH_2 at contact time 3 h, 25°C and 100 ppm. (b) The effect of pH media on the removal efficiency of BT and MO by magnetic MSNs-DTNB at contact time 3 h, 25°C and 100 ppm. (c) The effect of initial concentration on the removal efficiency of dyes by nanoadsorbents at contact time 3 h and 25°C.

The effect of time on the removal efficiency of BT and MO has been investigated at different exposure time, as shown in Figure 6. The removal efficiency increased gradually as the exposure time increased. No significant difference in the BT removal between magnetic MSNs-NH_2 and magnetic MSNs-DTNB. The maximum adsorption was obtained after 15 min exposure time. Magnetic MSNs-DTNB showed better adsorption capacity than magnetic MSNs-NH_2 for removing MO. The removal efficiency was ca. 100% in 15 min after contact time for magnetic MSNs-DTNB, whereas the removal efficiency was ~65% for magnetic MSNs-NH_2.

Pseudo-first-order and pseudo-second-order kinetic models were used to determine the adsorption mechanism of BT and MO onto magnetic MSNs-NH_2 and magnetic MSNs-DTNB. Figure 7 illustrates the plot curves of the adsorption data fitted with Pseudo-first-order and pseudo-second-order models. Table 3 shows the pseudo-first-order and pseudo-second-order kinetic models' constants for the adsorption of BT and MO by magnetic MSNs-NH_2 and magnetic MSNs-DTNB at 25°C. In both systems, the R^2 values for the first-order model were not high, as well as the estimated values of q_e from the model were different from the experimental values, suggesting that this model is not

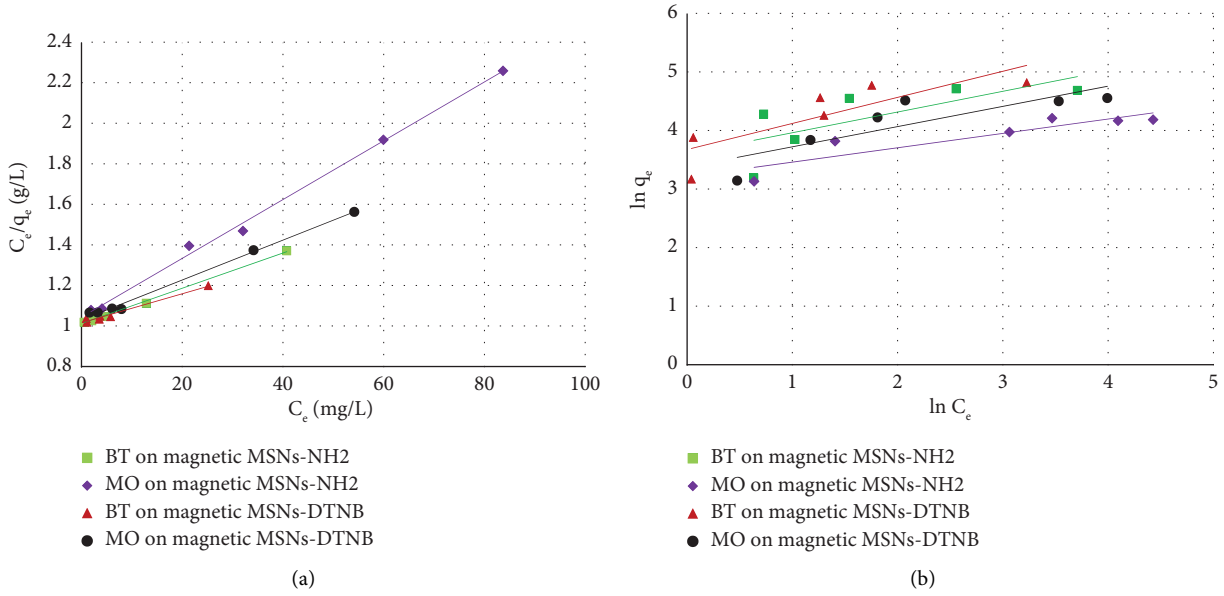

Figure 5: (a) Langmuir isotherm for the adsorption of BT and MO by magnetic MSNs-NH_2 and magnetic MSNs-DTNB at 25°C. (b) Freundlich isotherm for the adsorption of BT and MO by magnetic MSNs-NH_2 and magnetic MSNs-DTNB at contact time 3 h and 25°C.

Table 2: Langmuir and Freundlich isotherm parameters for the adsorption of BT and MO by magnetic MSNs-NH_2 and magnetic MSNs-DTNB at contact time 3 h and 25°C.

Material	Dye	Langmuir isotherm model			Freundlich isotherm model		
		q_{max} (mg/g^{-1})	K_L (L/mg^{-1})	R^2	n (L/mg^{-1})	K (mg/g^{-1})	R^2
Magnetic MSNs-NH_2	BT	115.13	0.008	0.993	2.83	37.23	0.518
	MO	68.93	0.014	0.996	4.07	25.12	0.811
Magnetic MSNs-DTNB	BT	139.27	0.007	0.979	2.24	39.85	0.701
	MO	101.62	0.010	0.995	2.89	29.55	0.714

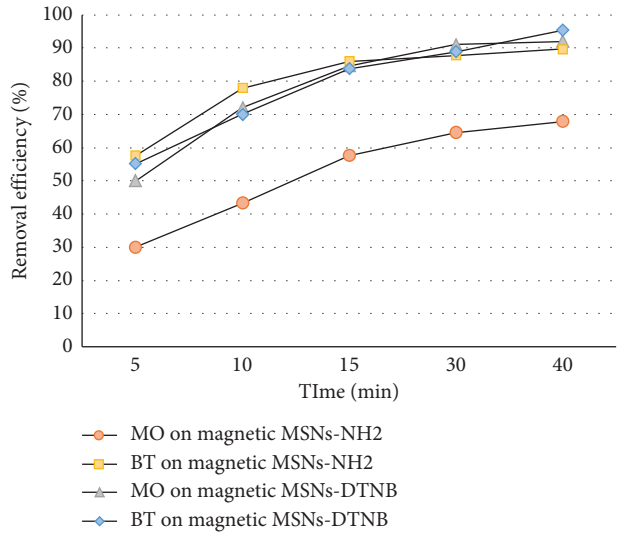

Figure 6: The effect of time on the removal efficiency of BT at pH 3 by magnetic MSNs-NH_2 and magnetic MSNs-DTNB at 25°C and 100 ppm. The effect of time on the removal efficiency of MO at pH 9 by magnetic MSNs-NH_2 and magnetic MSNs-DTNB at 25°C and 100 ppm.

appropriate to describe this adsorption process. When the experimental data was fitted with pseudo-second-order model, the R^2 values were nearly 1 and the calculated q_e were close to the experimental value, suggesting that the adsorption process in both systems followed the pseudo-second-order kinetic model.

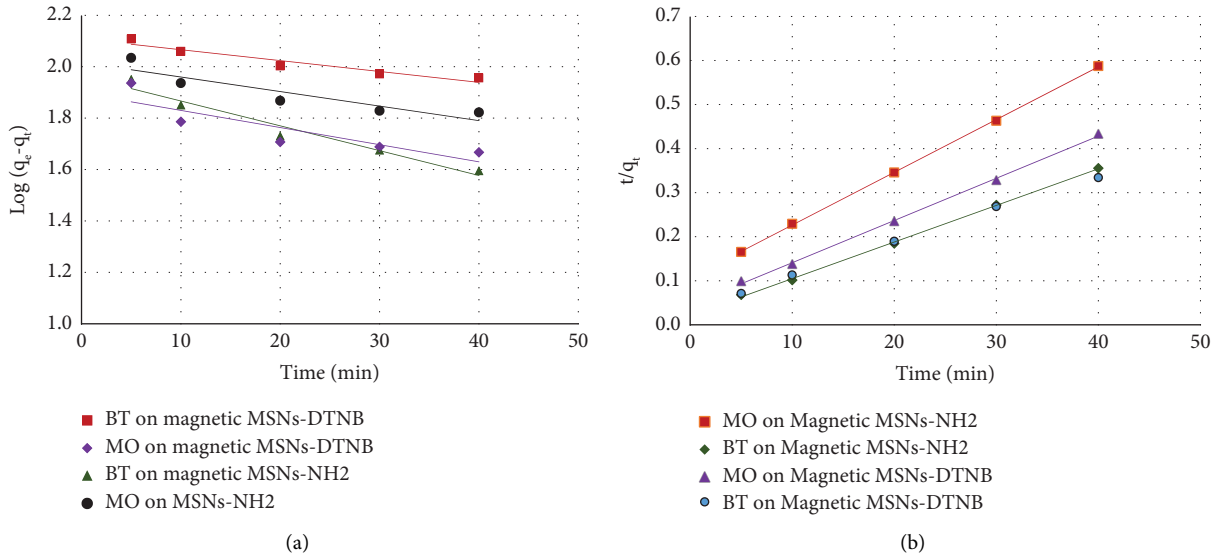

Figure 7: (a) Pseudo-first-order kinetics for the adsorption of BT and MO by magnetic MSNs-NH_2 and magnetic MSNs-DTNB at 25°C. (b) Pseudo-second-order kinetics for the adsorption of BT and MO by magnetic MSNs-NH_2 and magnetic MSNs-DTNB at 25°C.

Table 3: Pseudo-first-order and pseudo-second-order kinetic models' constants for the adsorption of BT and MO by magnetic MSNs-NH_2 and magnetic MSNs-DTNB at 25°C.

Material	Dye	Pseudo-first order			Pseudo-second order		
		q_e (mg/g^{-1})	k_1 (min^{-1})	R^2	q_e (mg/g^{-1})	k_2 (g.g^{-1}/min^{-1})	R^2
Magnetic MSNs-NH_2	BT	6.68	0.015	0.755	120.37	0.003	0.999
	MO	8.25	0.009	0.920	85.54	0.0013	0.999
Magnetic MSNs-DTNB	BT	7.14	0.022	0.954	132.35	0.0015	0.998
	MO	7.53	0.013	0.832	104.36	0.002	0.999

Table 4: Comparison of adsorption capacities of BT and MO dyes onto different adsorbents.

Adsorbent	Dye	q_e (mg/g^{-1})	References
Zeolites (S-1)	BT	17	[60]
Latvian sphagnum peat moss	BT	18	[61]
PMPC/BNC_2 nanocomposite	MO	4.5	[62]
Chitosan was coupled with succinimide (Ch/Su)	MO	10	[63]
Orange and lemon peels-derived activated carbon	MO	33	[64]
$MoSe_2$ microspheres	MO	37	[65]
ZnO-NPs	MO	65	[66]
Powder activated charcoal-supported TNTs (TNTs@PAC)	MO	107	[67]
Magnetic MSNs-DTNB	BT	139	In this work
Magnetic MSNs-DTNB	MO	102	In this work

The performance of fabricated nanoparticles toward removing BT and MO compared to other materials reported in the literature is illustrated in Table 4. It can be seen that magnetic MSNs-DTNB shows reasonable capacity which can be used as a good and inexpensive nanoadsorbent for organic dyes from contaminated water.

4. Conclusions

In this work, magnetic MSNs were prepared with an average size of 170 nm, with 20 nm Fe_3O_4 NPs embedded in MSPs' structure as determined by SEM and TEM images. The pore size of magnetic MSNs was estimated from the TEM image to be ca. 5 nm. After surface modification with amine, thiol groups were introduced to the surface via the reaction between amine and ethylene sulfide and reacted with 5,5′-dithiobis-(2-nitrobenzoic acid). FTIR spectra confirmed the successful attachment of DTNB molecules by appearance of peaks at ~1528 cm^{-1} and ~1365 cm^{-1}. The nanoadsorbents showed high removal efficiency towards removing BT and MO in acidic media. The percent adsorption of the adsorbent obtained was ca. 98% for both dyes at pH 3.0, the contact time was 2 h, and adsorbent dose was 10 mg. The maximum adsorption capacity by magnetic MSNs-DTNB

was obtained 139.27 mg/g (BT) and 101.62 mg/g (MO). The equilibrium data have been analyzed by Langmuir and Freundlich isotherm models. The linear regression coefficient value suggested that the adsorption of BT and MO onto nanoadsorbent followed the Langmuir isotherm among the tested models and second-order process. These findings suggested that the fabricated nanoadsorbents could be used to toxic ionic dyes from contaminated water effectively.

Data Availability

The data used to support the findings of this study are included within the article.

Conflicts of Interest

The authors declare that there are no conflicts of interest.

Acknowledgments

This research was supported by researchers supporting project number RSP2023R239, King Saud University, Riyadh, Saudi Arabia.

References

[1] V. S. Mane and P. Vijay Babu, "Kinetic and equilibrium studies on the removal of Congo red from aqueous solution using Eucalyptus wood (Eucalyptus globulus) saw dust," *Journal of the Taiwan Institute of Chemical Engineers*, vol. 44, no. 1, pp. 81–88, 2013.

[2] J. R. Deka, C.-L. Liu, T. H. Wang, W.-C. Chang, and H.-M. Kao, "Synthesis of highly phosphonic acid functionalized benzene-bridged periodic mesoporous organosilicas for use as efficient dye adsorbents," *Journal of Hazardous Materials*, vol. 278, pp. 539–550, 2014.

[3] C. Zhou, Q. Wu, T. Lei, and I. I. Negulescu, "Adsorption kinetic and equilibrium studies for methylene blue dye by partially hydrolyzed polyacrylamide/cellulose nanocrystal nanocomposite hydrogels," *Chemical Engineering Journal*, vol. 251, pp. 17–24, 2014.

[4] N. Delgado, A. Capparelli, A. Navarro, and D. Marino, "Pharmaceutical emerging pollutants removal from water using powdered activated carbon: study of kinetics and adsorption equilibrium," *Journal of Environmental Management*, vol. 236, pp. 301–308, 2019.

[5] H. Ali, E. Khan, and I. Ilahi, "Environmental chemistry and ecotoxicology of hazardous heavy metals: environmental persistence, toxicity, and bioaccumulation," *Journal of Chemistry*, vol. 2019, Article ID 6730305, 14 pages, 2019.

[6] B. Lellis, C. Z. Fávaro-Polonio, J. A. Pamphile, and J. C. Polonio, "Effects of textile dyes on health and the environment and bioremediation potential of living organisms," *Biotechnology Research and Innovation*, vol. 3, no. 2, pp. 275–290, 2019.

[7] R. Al-Tohamy, S. S. Ali, F. Li et al., "A critical review on the treatment of dye-containing wastewater: ecotoxicological and health concerns of textile dyes and possible remediation approaches for environmental safety," *Ecotoxicology and Environmental Safety*, vol. 231, Article ID 113160, 2022.

[8] Z. Aksu, "Application of biosorption for the removal of organic pollutants: a review," *Process Biochemistry*, vol. 40, no. 3-4, pp. 997–1026, 2005.

[9] J. Yun, Y. Wang, Z. Liu, Y. Li, H. Yang, and Z. L. Xu, "High efficient dye removal with hydrolyzed ethanolamine-Polyacrylonitrile UF membrane: rejection of anionic dye and selective adsorption of cationic dye," *Chemosphere*, vol. 259, Article ID 127390, 2020.

[10] M. D. Khan, A. Singh, M. Z. Khan, S. Tabraiz, and J. Sheikh, "Current perspectives, recent advancements, and efficiencies of various dye-containing wastewater treatment technologies," *Journal of Water Process Engineering*, vol. 53, Article ID 103579, 2023.

[11] S. Dutta, B. Gupta, S. K. Srivastava, and A. K. Gupta, "Recent advances on the removal of dyes from wastewater using various adsorbents: a critical review," *Materials Advances*, vol. 2, no. 14, pp. 4497–4531, 2021.

[12] Y. Yang, Y. Li, R. Mao et al., "Removal of phosphate in secondary effluent from municipal wastewater treatment plant by iron and aluminum electrocoagulation: efficiency and mechanism," *Separation and Purification Technology*, vol. 286, Article ID 120439, 2022.

[13] A. K. Badawi and K. Zaher, "Hybrid treatment system for real textile wastewater remediation based on coagulation/flocculation, adsorption and filtration processes: performance and economic evaluation," *Journal of Water Process Engineering*, vol. 40, Article ID 101963, 2021.

[14] P. N. Diagboya and E. D. Dikio, "Scavenging of aqueous toxic organic and inorganic cations using novel facile magneto-carbon black-clay composite adsorbent," *Journal of Cleaner Production*, vol. 180, pp. 71–80, 2018.

[15] P. N. Diagboya, B. I. Olu-Owolabi, D. Zhou, and B.-H. Han, "Graphene oxide–tripolyphosphate hybrid used as a potent sorbent for cationic dyes," *Carbon*, vol. 79, pp. 174–182, 2014.

[16] X. Li, L. Zhang, Z. Yang, P. Wang, Y. Yan, and J. Ran, "Adsorption materials for volatile organic compounds (VOCs) and the key factors for VOCs adsorption process: a review," *Separation and Purification Technology*, vol. 235, Article ID 116213, 2020.

[17] T. C. Costa, L. T. Hendges, B. Temochko et al., "Evaluation of the technical and environmental feasibility of adsorption process to remove water soluble organics from produced water: a review," *Journal of Petroleum Science and Engineering*, vol. 208, Article ID 109360, 2022.

[18] C. Du, Z. Zhang, G. Yu et al., "A review of metal organic framework (MOFs)-based materials for antibiotics removal via adsorption and photocatalysis," *Chemosphere*, vol. 272, Article ID 129501, 2021.

[19] Z. Anfar, H. Ait Ahsaine, M. Zbair et al., "Recent trends on numerical investigations of response surface methodology for pollutants adsorption onto activated carbon materials: a review," *Critical Reviews in Environmental Science and Technology*, vol. 50, no. 10, pp. 1043–1084, 2020.

[20] W. Xiao, X. Jiang, X. Liu et al., "Adsorption of organic dyes from wastewater by metal-doped porous carbon materials," *Journal of Cleaner Production*, vol. 284, Article ID 124773, 2021.

[21] N. S. Ali, N. M. Jabbar, S. M. Alardhi, H. S. Majdi, and T. M. Albayati, "Adsorption of methyl violet dye onto a prepared bio-adsorbent from date seeds: isotherm, kinetics, and thermodynamic studies," *Heliyon*, vol. 8, no. 8, Article ID e10276, 2022.

[22] A. Beagan, K. Alotaibi, M. Almakhlafi et al., "Amine and sulfonic acid functionalized mesoporous silica as an effective

adsorbent for removal of methylene blue from contaminated water," *Journal of King Saud University Science*, vol. 34, no. 2, Article ID 101762, 2022.

[23] A. M. Alswieleh, "Aspartic acid-and glycine-functionalized mesoporous silica as an effective adsorbent to remove methylene blue from contaminated water," *Journal of Chemistry*, vol. 2022, Article ID 5375815, 14 pages, 2022.

[24] K. Khezri, H. Roghani-Mamaqani, M. Sarsabili, M. Sobani, and S.-A. Mirshafiei-Langari, "Spherical mesoporous silica nanoparticles/tailor-made polystyrene nanocomposites by in situ reverse atom transfer radical polymerization," *Polymer Science-Series B*, vol. 56, no. 6, pp. 909–918, 2014.

[25] R. A. Melo, M. V. Giotto, J. Rocha, and E. A. Urquieta-González, "MCM-41 ordered mesoporous molecular sieves synthesis and characterization," *Materials Research*, vol. 2, no. 3, pp. 173–179, 1999.

[26] D. Zhao, J. Feng, Q. Huo et al., "Triblock copolymer syntheses of mesoporous silica with periodic 50 to 300 angstrom pores," *Science*, vol. 279, no. 5350, pp. 548–552, 1998.

[27] N. S. Ali, Z. T. Alismaeel, H. S. Majdi et al., "Modification of SBA-15 mesoporous silica as an active heterogeneous catalyst for the hydroisomerization and hydrocracking of n-heptane," *Heliyon*, vol. 8, no. 6, 2022.

[28] S. Hozhabr Araghi, M. H. Entezari, and M. Chamsaz, "Modification of mesoporous silica magnetite nanoparticles by 3-aminopropyltriethoxysilane for the removal of Cr (VI) from aqueous solution," *Microporous and Mesoporous Materials*, vol. 218, pp. 101–111, 2015.

[29] J. Wu, P. Su, J. Huang, S. Wang, and Y. Yang, "Synthesis of teicoplanin-modified hybrid magnetic mesoporous silica nanoparticles and their application in chiral separation of racemic compounds," *Journal of Colloid and Interface Science*, vol. 399, pp. 107–114, 2013.

[30] S. Laurent, D. Forge, M. Port et al., "Magnetic iron oxide nanoparticles: synthesis, stabilization, vectorization, physicochemical characterizations, and biological applications," *Chemical Reviews*, vol. 108, no. 6, pp. 2064–2110, 2008.

[31] D. Ling and T. Hyeon, "Chemical design of biocompatible iron oxide nanoparticles for medical applications," *Small*, vol. 9, no. 10, pp. 1450–1466, 2013.

[32] A. Grau-Atienza, E. Serrano, N. Linares, P. Svedlindh, G. Seisenbaeva, and J. García-Martínez, "Magnetically separable mesoporous Fe3O4/silica catalysts with very low Fe3O4 content," *Journal of Solid State Chemistry*, vol. 237, pp. 138–143, 2016.

[33] T. A. Arica, E. Ayas, and M. Y. Arica, "Magnetic MCM-41 silica particles grafted with poly (glycidylmethacrylate) brush: modification and application for removal of direct dyes," *Microporous and Mesoporous Materials*, vol. 243, pp. 164–175, 2017.

[34] P. Yuan, D. Liu, M. Fan et al., "Removal of hexavalent chromium [Cr (VI)] from aqueous solutions by the diatomite-supported/unsupported magnetite nanoparticles," *Journal of Hazardous Materials*, vol. 173, no. 1-3, pp. 614–621, 2010.

[35] P. S. Mueller, C. P. Parker, and S. C. Larsen, "One-pot synthesis of iron oxide mesoporous silica core/shell nanocomposites," *Microporous and Mesoporous Materials*, vol. 204, pp. 173–179, 2015.

[36] J. Liu, S. Z. Qiao, Q. H. Hu, and G. Q. Max Lu, "Magnetic nanocomposites with mesoporous structures: synthesis and applications," *Small*, vol. 7, no. 4, pp. 425–443, 2011.

[37] X. Yao, X. Niu, K. Ma et al., "Graphene quantum dots-capped magnetic mesoporous silica nanoparticles as a multifunctional platform for controlled drug delivery, magnetic hyperthermia, and photothermal therapy," *Small*, vol. 13, no. 2, Article ID 1602225, 2017.

[38] Y. Zhang, Z. Su, B. Li, L. Zhang, D. Fan, and H. Ma, "Recyclable magnetic mesoporous nanocomposite with improved sensing performance toward nitrite," *ACS Applied Materials and Interfaces*, vol. 8, no. 19, pp. 12344–12351, 2016.

[39] J. Gao, H. Yu, L. Zhou, Y. He, L. Ma, and Y. Jiang, "Formation of cross-linked nitrile hydratase aggregates in the pores of tannic-acid-templated magnetic mesoporous silica: characterization and catalytic application," *Biochemical Engineering Journal*, vol. 117, pp. 92–101, 2017.

[40] S. Liu, C. Deng, and X. Zhang, "Facile synthesis of Cu2+-modified mesoporous silica-coated magnetic graphene composite for enrichment of microcystin-LR followed by mass spectrometry analysis," *Talanta*, vol. 154, pp. 183–189, 2016.

[41] J. Dai, J. He, A. Xie et al., "Novel pitaya-inspired well-defined core–shell nanospheres with ultrathin surface imprinted nanofilm from magnetic mesoporous nanosilica for highly efficient chloramphenicol removal," *Chemical Engineering Journal*, vol. 284, pp. 812–822, 2016.

[42] Z. Qiang, X. Bao, and W. Ben, "MCM-48 modified magnetic mesoporous nanocomposite as an attractive adsorbent for the removal of sulfamethazine from water," *Water Research*, vol. 47, no. 12, pp. 4107–4114, 2013.

[43] T. K. Mahto, S. Chandra, C. Haldar, and S. K. Sahu, "Kinetic and thermodynamic study of polyaniline functionalized magnetic mesoporous silica for magnetic field guided dye adsorption," *RSC Advances*, vol. 5, no. 59, pp. 47909–47919, 2015.

[44] K. M. Alotaibi, A. A. Almethen, A. M. Beagan et al., "Quaternization of poly (2-diethyl aminoethyl methacrylate) brush-grafted magnetic mesoporous nanoparticles using 2-Iodoethanol for removing anionic dyes," *Applied Sciences*, vol. 11, no. 21, Article ID 10451, 2021.

[45] R. Das, V. S. Sypu, H. K. Paumo, M. Bhaumik, V. Maharaj, and A. Maity, "Silver decorated magnetic nanocomposite (Fe3O4@ PPy-MAA/Ag) as highly active catalyst towards reduction of 4-nitrophenol and toxic organic dyes," *Applied Catalysis B: Environmental*, vol. 244, pp. 546–558, 2019.

[46] D. Liu, J.-H. Lei, L.-P. Guo, X.-D. Du, and K. Zeng, "Ordered thiol-functionalized mesoporous silica with macrostructure by true liquid crystal templating route," *Microporous and Mesoporous Materials*, vol. 117, no. 1-2, pp. 67–74, 2009.

[47] E. M. Usai, M. F. Sini, D. Meloni, V. Solinas, and A. Salis, "Sulfonic acid-functionalized mesoporous silicas: microcalorimetric characterization and catalytic performance toward biodiesel synthesis," *Microporous and Mesoporous Materials*, vol. 179, pp. 54–62, 2013.

[48] J. R. Deka, D. Saikia, Y.-S. Lai, C.-H. Tsai, W.-C. Chang, and H.-M. Kao, "Roles of nanostructures and carboxylic acid functionalization of ordered cubic mesoporous silicas in lysozyme immobilization," *Microporous and Mesoporous Materials*, vol. 213, pp. 150–160, 2015.

[49] A. M. Beagan, "Investigating methylene blue removal from aqueous solution by cysteine-functionalized mesoporous silica," *Journal of Chemistry*, vol. 2021, Article ID 8839864, 12 pages, 2021.

[50] A. M. Alswieleh, H. Y. Albahar, A. M. Alfawaz et al., "Evaluation of the adsorption efficiency of glycine-iminodiacetic acid-and amino propyl-functionalized silica nanoparticles for the removal of potentially toxic elements from contaminated water solution," *Journal of Nanomaterials*, vol. 2021, Article ID 6664252, 12 pages, 2021.

[51] A. M. Alswieleh, "Cysteine-and glycine-functionalized mesoporous silica as adsorbents for removal of paracetamol from aqueous solution," *International Journal of Environmental Analytical Chemistry*, vol. 103, no. 9, pp. 2004–2015, 2021.

[52] A. M. Beagan, "Potential efficiency of magnetic mesoporous silica nanoparticles modified with aspartic acid to cationic dye removal from aqueous solution," *International Journal of Environmental Analytical Chemistry*, pp. 1–14, 2022.

[53] A. Beagan, R. Alshammari, L. Alotaibi, H. Albarrak, K. Alotaibi, and A. Alswieleh, "High-efficient anionic dyes removal from water by cationic polymer brush functionalized magnetic mesoporous silica nanoparticles," *Processes*, vol. 10, no. 8, p. 1565, 2022.

[54] P. N. Diagboya, B. I. Olu-Owolabi, and K. O. Adebowale, "Synthesis of covalently bonded graphene oxide–iron magnetic nanoparticles and the kinetics of mercury removal," *RSC Advances*, vol. 5, no. 4, pp. 2536–2542, 2015.

[55] A. M. Beagan, A. A. Alghamdi, S. S. Lahmadi et al., "Folic acid-terminated poly (2-diethyl amino ethyl methacrylate) brush-gated magnetic mesoporous nanoparticles as a smart drug delivery system," *Polymers*, vol. 13, no. 1, p. 59, 2020.

[56] A. Alfawaz, K. Alzahrani, A. Niazy et al., "Smart nanocarrier based on poly (oligo (ethylene glycol) methyl ether acrylate) terminated pH-responsive polymer brushes grafted mesoporous silica nanoparticles," *Applied Sciences*, vol. 12, no. 7, p. 3688, 2022.

[57] S. Mu, Y. Liu, T. Wang et al., "Unsaturated nitrogen-rich polymer poly (l-histidine) gated reversibly switchable mesoporous silica nanoparticles using "graft to" strategy for drug controlled release," *Acta Biomaterialia*, vol. 63, pp. 150–162, 2017.

[58] N. Rasool, D. Negi, and Y. Singh, "Thiol-Functionalized, Antioxidant, and Osteogenic Mesoporous Silica Nanoparticles for Osteoporosis," *ACS Biomaterials Science & Engineering*, vol. 9, 2023.

[59] P. N. Diagboya, B. I. Olu-Owolabi, and K. O. Adebowale, "Microscale scavenging of pentachlorophenol in water using amine and tripolyphosphate-grafted SBA-15 silica: batch and modeling studies," *Journal of Environmental Management*, vol. 146, pp. 42–49, 2014.

[60] A. Tabti, I. Benchikh, M. Serier, F. Launay, and F. Djafri, "Adsorption of bromothymol blue (BTB) dye using four zeolites as adsorbent," *Kemija u Industriji*, vol. 70, no. 5-6, pp. 243–250, 2021.

[61] S. H. Lubbad, B. K. Abu Al-Roos, and F. S. Kodeh, "Adsorptive-removal of bromothymol blue as acidic-dye probe from water solution using Latvian sphagnum peat moss: thermodynamic assessment, kinetic and isotherm modeling," *Current Green Chemistry*, vol. 6, no. 1, pp. 53–61, 2019.

[62] C. Vilela, C. Moreirinha, A. Almeida, A. J. Silvestre, and C. S. Freire, "Zwitterionic nanocellulose-based membranes for organic dye removal," *Materials*, vol. 12, no. 9, p. 1404, 2019.

[63] S. Aboulhadeed, H. Ahmed, R. Khalifa et al., "Methyl orange dye removal from wastewater by novel developed chitosan Schiff bases," *Desalination and Water Treatment*, vol. 244, pp. 279–290, 2021.

[64] D. Ramutshatsha-Makhwedzha, A. Mavhungu, M. L. Moropeng, and R. Mbaya, "Activated carbon derived from waste orange and lemon peels for the adsorption of methyl orange and methylene blue dyes from wastewater," *Heliyon*, vol. 8, no. 8, 2022.

[65] H. Tang, H. Huang, X. Wang, K. Wu, G. Tang, and C. Li, "Hydrothermal synthesis of 3D hierarchical flower-like MoSe2 microspheres and their adsorption performances for methyl orange," *Applied Surface Science*, vol. 379, pp. 296–303, 2016.

[66] M. N. Zafar, Q. Dar, F. Nawaz, M. N. Zafar, M. Iqbal, and M. F. Nazar, "Effective adsorptive removal of azo dyes over spherical ZnO nanoparticles," *Journal of Materials Research and Technology*, vol. 8, no. 1, pp. 713–725, 2019.

[67] Y. Lin, J. Ma, W. Liu, Z. Li, and K. He, "Efficient removal of dyes from dyeing wastewater by powder activated charcoal/titanate nanotube nanocomposites: adsorption and photoregeneration," *Environmental Science and Pollution Research*, vol. 26, no. 10, pp. 10263–10273, 2019.